Size-Dependent Endocytosis of Nanoparticles

By *Sulin Zhang,* Ju Li, George Lykotrafitis, Gang Bao,* and *Subra Suresh*

Recent advances in nanotechnology have stimulated novel applications in biomedicine where nanoparticles (NPs) are used to achieve drug delivery and photodynamic therapy. In chemotherapeutic cancer treatment, tumor-specific drug delivery is a topic of considerable research interest for achieving enhanced therapeutic efficacy and for mitigating adverse side effects. Most anticancer agents are incapable of distinguishing between benign and malignant cells, and consequently cause systematic toxicity during cancer treatment. Owing to their small size, ligand-coated NPs can be efficiently directed toward, and subsequently internalized by tumor cells through ligand–receptor recognition and interaction (see Fig. 1), thereby offering an effective approach for specific targeting of tumor cells. For example, branching dendrimers have recently been identified as potential candidates for site-specific drug carriers.[2] NPs have also been exploited in other biomedical applications such as bioimaging[3,4] and biosensing.[5,6] It has been demonstrated that florescent quantum dots are efficient in tumor cell imaging, recognition, and tracking,[3,4] and that gold NPs are capable of detecting small proteins.[5,6] To enable rational design of such NP-based agents, it is essential to understand the underlying mechanisms that govern the transmembrane transport and invagination of NPs in biological cells. In this communication, we present a thermodynamic model for receptor-mediated endocytosis of ligand-coated NPs. We identify an optimal NP radius at which the cellular uptake reaches a maximum of several thousand at physiologically relevant parameters, and we show that the cellular uptake of NPs is regulated by membrane tension, and can be elaborately controlled by particle size. The optimal NP radius for endocytosis is on the order of 25–30 nm, which is in good agreement with prior estimates.[7]

Theoretical models[7–11] have provided insights into the dynamics of receptor-mediated endocytosis based on energetic and kinetic considerations, primarily in the context of virus budding. Lerner et al.[8] argued that the discreteness of membrane wrapping via ligand-receptor binding results in a corrugated energy landscape for NP wrapping, which governs the kinetics of endocytosis. In contrast, Gao et al.[7] proposed that the endocytic rate is limited by the diffusion of receptors toward the NP. They predicted that NPs with a radius of approximately 25 nm have the shortest internalization time of about 20 minutes, which appears to be consistent with certain experimental data.[12–14]

The aforementioned models have attempted to rationalize the mechanisms of receptor-mediated endocytosis from a kinetic point of view and have sought to address the question of ''how fast'' a single NP can be transported into the cell. In this work, we address an equally important question to the realization of NP-based cell type-specific targeting units, namely, ''how many'' NPs can be endocytosed in a sufficiently long period? The question is important for a range of medical and biological applications of NPs, including the maximum numbers of proteins tagged when NPs are used to protein targeting, and the maximum drug-delivery capability when NPs are used to internalize drug molecules. We approach the problem from a different viewpoint by invoking thermodynamic arguments. In order to develop a quantitative framework for this problem, we consider a cell immersed in a solution with dispersed ligand-coated NPs. Driven by the chemical potential difference of the adherent and suspended NPs, the many-NP-cell system reaches a thermodynamic equilibrium at which a certain number of NPs are endocytosed. The existence of the thermodynamic equilibrium is suggested by recent experiments where the cellular uptake of NPs increases at the initial stage of cell incubation, and

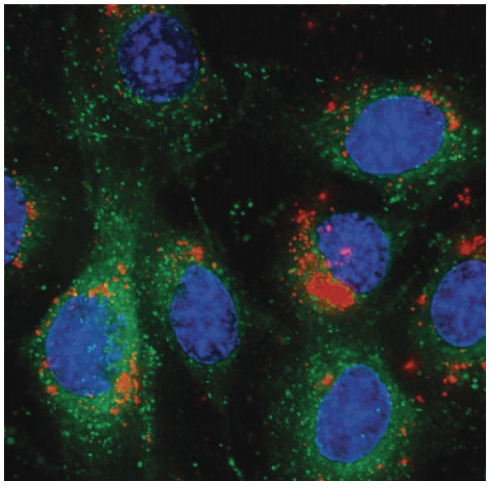

Figure 1. Confocal fluorescent images of 9L glioma cells.[1] The cellular membranes are green and the nuclei are blue. Red dots are iron oxide nanoparticles functionalized with chlorotoxin, a glioma tumor-targeting molecule, and the near-infrared fluorophore Cy5.5. Reproduced with permission from [1]. Copyright 2005 American Chemical Society.

[*] Prof. S. Zhang
Department of Engineering Science and Mechanics
The Pennsylvania State University
University Park, PA 16802 (USA)
E-mail: suz10@psu.edu
Prof. J. Li
Department of Materials Science and Engineering
University of Pennsylvania
Philadelphia, PA 19104 (USA)
Dr. G. Lykotrafitis, Prof. S. Suresh
Department of Materials Science and Engineering
Massachusetts Institute of Technology
Cambridge, MA 02139 (USA)
Prof. G. Bao
Department of Biomedical Engineering
Georgia Institute of Technology and Emory University
Atlanta, GA 30332 (USA)

DOI: 10.1002/adma.200801393

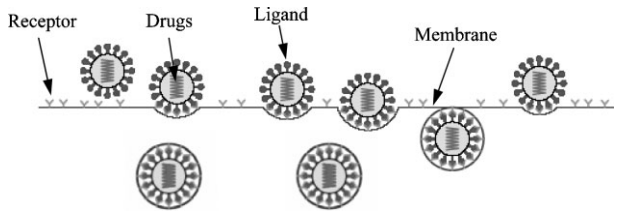

Figure 2. Schematics of adhering NPs wrapped by cell membrane with different degrees of wrapping; some are endocytosed.

reaches a plateau within several hours.[15,16] In experiments, NP density in the bulk solution is taken as an adjustable parameter that thermodynamically controls the number of adsorbed NPs onto the cell membrane.[11,17] Consideration of the detailed mechanisms of this adsorption process itself is beyond the scope of the present study. Instead, we assume that depletion of NPs in the vicinity right outside a cell can be ignored and N NPs adhere to the cell surface through specific interactions via reversible ligand–receptor binding. Upon attaining thermodynamic equilibrium, the N NPs are wrapped by the cell membrane with different degrees of wrapping; some of them are fully wrapped and endocytosed, as schematically shown in Figure 2. We assume that a finite number of receptors exists on the cell membrane, with an average density ξ_0. We denote the cross-sectional area of the receptor A_0, and hereafter use it as unit area. Correspondingly, $L \sim \sqrt{A_0}$ is taken as unit length. For a typical transmembrane receptor, $L \approx 15$ nm.[10] The NPs are assumed to be spherical in shape and coated with ligands on their surfaces. For a given radius of NPs, R, the maximum number of receptors accessible by an NP is $K = 4\pi R^2/A_0$; K is also the surface area of the NP in the unit of A_0. The ligands coated on the NP surface are assumed to be immobile and specific to the transmembrane receptors, while the receptors are free to diffuse on the cell membrane. We denote by M the total area of the plasma membrane of a cell (in the unit of A_0) to which NPs adhere; M is therefore regarded as the total number of sites accessible by receptors. The surface concentration of NPs is then $c = N/M$. We characterize the degree of wrapping by the fraction of wrapped area, $\eta = k/K$. Thus, $\eta = 0$ corresponds to the completely naked state, $\eta = 1$ to the fully wrapped state, and $0 < \eta < 1$ to the partially wrapped state. The wrapped area k is treated as an integer in the range of $[0, K]$, in accordance to the discrete nature of wrapping: each binding of a ligand–receptor pair corresponds to a unit area advance of wrapping.

When binding occurs between a ligand–receptor pair, the released chemical energy μ drives the local wrapping of the membrane around a NP at the cost of elastic deformation energy of the membrane. According to the classical Canham–Helfrich theory,[18] the elastic-deformation energy includes the bending energy due to curvature formation and the stretching energy due to lateral membrane tension. At a specified degree of wrapping η, the bending and stretching energies stored in the membrane segment adhering to the NP are $8\pi\kappa\eta$ and $k\eta\sigma$, respectively,[19] where κ is the normal bending rigidity with units of energy and σ is the membrane tension. For partially wrapped NPs ($0 < \eta < 1$), the strongly curved membrane detaching from the contact of the NP contributes an additional deformation energy Λ, which was found to depend on two dimensionless variables,[19] η and $\tilde{\sigma} = \sigma R^2/\kappa$, i.e., $\Lambda = \Lambda(\eta; \tilde{\sigma})$. As η reaches a critical value close to unity, the highly curved free membrane is energetically unfavorable.[20] As a result, pinch-off reaction takes place, followed by the host membrane fusion. The pinch-off reaction results in a topology change of the configuration which, according to the Gauss–Bonnet theorem, leads to an increase of $4\pi\bar{\kappa}$ in Gaussian bending energy, with $\bar{\kappa}$ representing the Gaussian bending rigidity of the cell membrane.

At thermodynamic equilibrium, the receptors are partitioned into two groups. The receptors in the first group are diffusible within the free membrane regions, while the receptors in the second group are densely packed on NP surfaces via ligand–receptor binding, forming curved membrane regions that wrap the NPs with different degrees of wrapping. To describe the wrapping-size distribution of N NPs, we adopt the notations set by Tzlil et al.,[10] and denote by n_k the number of NPs whose wrapped area is k. Thus,

$$N = \sum_{k=0}^{K} n_k. \tag{1}$$

Note that the state $k = K$ corresponds to the endocytosed state. Therefore, the subgroups considered in Equation 1 include both internalized NPs and NPs on cell surface. The total bound area M_b is

$$M_b = \sum_{k=0}^{K} k n_k, \tag{2}$$

leaving out a free membrane area $M_f = M - M_b$.

Corresponding to the wrapping-size distribution of NPs described in Equation 1, a total free energy functional for the many-NP-cell system takes the following form:

$$\begin{aligned} W = {} & M_f[\xi_f \ln \xi_f + (1-\xi_f)\ln(1-\xi_f)] \\ & + M_b[\xi_b \ln \xi_b + (1-\xi_b)\ln(1-\xi_b)] \\ & + \textstyle\sum n_k[\ln n_k/M - 1] - \mu L_b + \hat{\kappa} M_b \\ & + \textstyle\sum n_k(\Lambda_k + \Gamma_k) + 4\pi\bar{\kappa} n_K \end{aligned} \tag{3}$$

where ξ_b and ξ_f represent the densities of the bound and free receptors, respectively. By definition, $\xi_b = L_b/M_b$ and $\xi_f = L_f/M_f$, where L_b and L_f are the numbers of bound and free receptors, respectively. In the above free energy functional (and hereafter), all the energy quantities are denoted in units of the thermal energy $k_B T$. The first three terms are entropic contributions: the first two terms are the translational entropies of the bound and free receptors, respectively, and the third term accounts for the configurational entropy of the 2D mixture of wrapped NPs, treated here as a multicomponent ideal gas. The next four terms are energetic contributions: $-\mu L_b$ is the chemical energy release upon the binding of L_b ligand–receptor pairs; $\hat{k} M_b$ is the total bending energy, where $\hat{k} = 8\pi\kappa/K$ is the bending energy density (per unit area). The third energetic term lumps over the stretching energy of the bound membrane $\Gamma_k = k\eta\sigma$ and the energy Λ_k of the curved free membrane detaching from the NP. The energy Λ_k is

evaluated based on the assumption that the spacing between neighboring NPs is sufficiently large so that their elastic deformation fields only weakly interact with each other. Numerically determining Λ_k involves solving a series of ordinary differential equations using the shooting method.[19] The last term accounts for the energy variation caused by the topological change due to pinch-off reaction.

The choice of the parameters involved in the thermodynamic model is guided by experimental data whenever possible. The bending rigidity κ is typically on the order of $20k_BT$.[18] The ligand-receptor binding energy μ is assumed to be comparable to the typical antibody–antigen interaction, which is also on the order of $20k_BT$.[21] Experiments have revealed that endocytosis may be clathrin-dependent, where clathrin coats generate a membrane curvature for wrapping of NPs. The present model is applicable to both clathrin-dependent and clathrin-free endocytic mechanisms. For the former case, the effects of clathrin coats can be included by regarding the energy supplied by clathrin coats as a part of the ligand–receptor binding energy. The density of the receptors is typically 100–400 receptors per μm^2.[22,23] Converting to the present units, ξ_0 ranges from 0.02 to 0.1. We note that the receptors internalized by NP endocytosis may be recycled back to the host membrane; they may also be degraded in the endosomes and lysosomes. In addition, new receptors may be produced and diffuse to the cell membrane. The precise amount of receptors involved in these processes is currently unknown. In the present study, we assume that ξ_0 is a constant. However, we anticipate that these effects can be appropriately incorporated in the theoretical model through a parametric study of the density of receptors on cell membrane. Due to lack of sufficient experimental data, the Gaussian bending rigidity $\bar{\kappa}$ is unknown, and here taken to be zero unless otherwise mentioned. One should note, however, that the value of $\bar{\kappa}$ directly influences the energetics at the endocytosed state, since a negative (positive) Gaussian bending rigidity promotes (resists) endocytosis. Membrane tension calculated from the tether force spans several orders of magnitude, ranging from $7.5 \times 10^{-4}\ k_BT/nm^2$ to $0.25\ k_BT/nm^2$ across all the regions of the plasma membrane.[24] Besides the in-plane tension, a significant portion (~75%) of the apparent membrane tension is attributed to membrane–cytoskeleton adhesion.[25] Surface concentration of NPs is controllable by the NP density in the bulk solution. In our simulations, c ranges from 0.001 to 0.005, which corresponds to sparse packing for small particles ($K = 20$) but rather dense packing for large particles ($K = 250$). Finally, given that the diameter of a cell is typically on the order of 15 μm,[15,16] the area of plasma membrane that encloses the cell is approximately $707\ \mu m^2$ ($M = 3.14 \times 10^6$). In the succeeding discussion, we choose $\kappa = 20k_BT$, $\mu = 20k_BT$, $c = 0.003$, $\xi_0 = 0.05$, $\sigma = 0.001k_BT/nm^2$, and $M = 3.14 \times 10^6$, unless otherwise specified.

We next present our numerical results. Figure 3 shows a set of key results of this article, which indicate that the cellular uptake is strongly dependent on the particle size. The solid line in Figure 3 is computed with the parametric values described above. For the range of the particle radius studied (20–60 nm), we identify three regimes separated by two characteristics NP radii, R_{min} and R_{max}. In region I ($R < R_{min} \approx 22$ nm), endocytosis hardly occurs; in region III ($R > R_{max} = 60$ nm), the cellular uptake is rather small

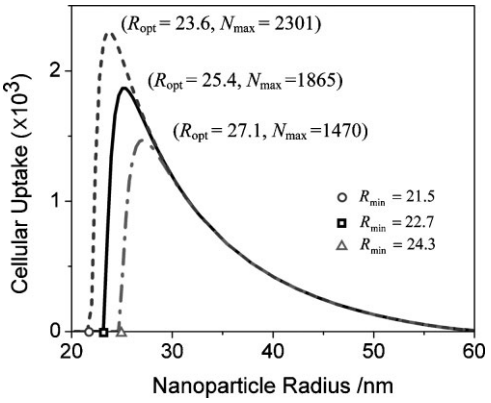

Figure 3. Size-dependent cellular uptake of NPs characterized by two typical radii: R_{min} and R_{max}. In region I ($R < R_{min}$), endocytosis hardly occurs; in region III ($R > R_{max} = 60$ nm), endocytosis rarely occurs. In region II ($R_{min} < R < R_{max}$), an optimal NP radius R_{opt} is identified at which the uptake ratio is maximized. For biologically reasonable parameters, $\kappa = 20k_BT$ and $\mu = 20k_BT$, $R_{min} \approx 22$ nm, $R_{opt} \approx 25.4$ nm, and the maximal cellular uptake is $N_{max} = 1865$. Changing the values of κ and μ shifts R_{min} and R_{opt}, but not R_{max}. A larger μ ($22k_BT$, dashed line) yields a smaller optimal radius ($R_{opt} = 23.6$nm) and a higher maximal cellular uptake ($N_{max} = 2301$). Conversely, a smaller μ ($18k_BT$, dash-dotted line) yields a larger optimal radius ($R_{opt} = 27.1$ nm) but a lower maximal cellular uptake ($N_{max} = 1470$).

(e.g., at $R = 60$ nm, the cellular uptake is only ~10); in region II ($R_{min} < R < R_{max}$), we identified an optimal NP radius $R_{opt} \approx 25$ nm, at which the internalization reaches a maximum $N_{max} = 1865$ for a cell with surface area of $\sim 707\ \mu m^2$. We note that cellular uptake depends on the relative values of κ and μ when the particle radius is relatively small ($R < 30$). Accordingly, R_{min} and R_{opt} change slightly if either of these two values (κ and μ) varies within several k_BT, while R_{max} remains almost the same. In addition, a smaller ligand–receptor binding energy lowers the cellular uptake. For example, changing μ by $2k_BT$ but keeping κ at $20k_BT$, we found that both R_{min} and R_{opt} shift by ~2 nm. A larger μ ($22k_BT$, dashed line in Fig. 3) yields a smaller optimal radius and a higher maximal cellular uptake. Conversely, a smaller μ ($18k_BT$, dash-dotted line) yields a larger optimal radius but a lower maximal cellular uptake. Considering the commonly accepted range for μ, from $15k_BT$ to 20 k_BT, the optimal particle radius changes from 25.4 nm to 30.2 nm. In contrast, the receptor density ξ_0 sensitively affects the cellular uptake, but not the characteristic radii. The maximal cellular uptake increases by ~32% (from 1865 to 2468) when ξ_0 is doubled. Given the biologically reasonable range of receptor density and other relevant parameters, the maximal cellular uptake ranges approximately from 500 to 5000.

The vanishing cellular uptake in region I ($R < R_{min}$) can be rationalized by examining the *local* energetics of a single-NP wrapping. We begin by temporarily setting aside the translational entropy of the receptors, and exclusively balance the adhesion energy with the bending energy (stretching energy is small for small NPs). Wrapping proceeds only if the adhesion energy density exceeds the bending energy density. For $\kappa = 20k_BT$ and $\mu = 20k_BT$, the local energetic requirement dictates the lower

bound of NP radius $R_{min} = \sqrt{2\kappa A_0/\mu} \approx 22$ nm, below which endocytosis does not occur due to excessive bending energy penalty. In other words, the adhesion energy cannot sufficiently compensate for the bending energy. The existence of such a lower bound value of the particle radius was suggested by a recent experiment of Chithrani et al.,[16] who observed that endocytosis of gold NPs of 7 nm in radius into mammalian cells (see Table 1) can only occur when at least six of them cluster together. This cluster radius is roughly on the order of ~20 nm, which agrees with our model prediction.

The very low cellular uptake in region III ($R > R_{max}$) can be understood by examining the *global* energetics of multiple NP wrapping. One notes that the total adhesion and bending energies depend only on the total wrapping area, regardless of whether this area is allocated to a few fully wrapped NPs or to many partially wrapped NPs. The argument above suggests that the adhesion and bending energies together feature a flat energy landscape of wrapping (without any energy wells), which favors a broad wrapping-size distribution and gives no preference to the formation of either partially or fully wrapped NPs. In contrast, energy terms associated with membrane tension (Γ_k and Λ_k) are nonlinear functions of the degree of wrapping η. At small particle radii ($R < R_{min}$), the two energy terms associated with membrane tension are rather small, and the balance between the adhesion and bending energies completely accounts for the cellular uptake. At the optimal particle radius, these energy terms associated with membrane tension modify the flat energy landscape into a double-well energy landscape, favoring (at least locally) both the completely naked and fully wrapped states, with a bias to the former (see Fig. 1a in the Supporting Information). Besides accounting for the energy penalty arising from curvature, the ligand–receptor binding energy also needs to surmount the thermodynamic energy barrier for endocytosis, arising from membrane tension. The barrier at the optimal radius is relatively small, and thus the cellular uptake is high. The bias to the completely naked state is increasingly more pronounced as the membrane tension increases. At a sufficiently large particle radius, the thermodynamic barrier becomes significant. To overcome the energy barrier, NPs compete for receptors during endocytosis, manifested as the rapid depletion of the free receptors on the cell membrane with increasing particle radius (see Fig. 2 in the Supporting Information). We found that when the particle radius approaches to 60 nm, the source-limiting endocytic mechanism shuts down further endocytosis, since almost all the free receptors are used out.

In a series of experimental studies, Chithrani et al.[15,16] examined the cellular uptake of protein-coated spherical and rod-shaped gold NPs by HeLa cells, which are ovarian cancer cells, SNB19 cells, which are brain tumor cells, and STO cells, which are fibroblast cells. They observed that cells take up spherical NPs more efficiently than rod-shaped ones. For spherical NPs, they reported an optimal particle radius of ~25 nm, at which the cellular uptake reaches a maximum independent of the cell lines. The cellular uptake at the optimal particle radius reported by Chithrani et al.[16] ranges from 500 to 6000 depending on the types of cell lines and of the proteins coated onto the particles. Both the optimal particle radius (25–30 nm) and the maximal cellular uptake (500–5000) predicted by the present model are quantitatively consistent with the experimental results reported by Chithrani et al. (see Table 1).

The thermodynamic framework established here allows us to probe the regulation role of membrane tension on the cellular uptake. Membrane tension of living cells reported in literature spans several orders of magnitude.[24] Here, we vary the membrane tension in a wide range, although it should be noted that extremely large values result in structural failure of the bilayer. Using an energetic argument similar to that invoked before for the wrapping of multiple NPs, one notes that, at a fixed particle radius, the energy landscape of NP wrapping is flat at zero membrane tension (favoring a broad wrapping size distribution), modified to a double-well energy landscape at intermediate membrane tension, and finally to a single-well energy profile at sufficiently large membrane tension. The characteristic membrane-tension-mediated energy landscape, along with the competition of receptors among NPs, governs the cellular uptake. Figure 4a shows the maximal cellular uptake at the optimal particle radius as a function of membrane tension (the optimal particle radius depends only weakly on membrane tension). At zero membrane tension, the uptake ratio is quite small, due to the broad wrapping-size distribution. The cellular uptake rapidly increases with increasing membrane tension and it reaches a peak, beyond which the cellular uptake gradually decreases to zero. One notes from Figure 4a that the cellular uptake remains at a relatively high level within a rather narrow range of membrane tension, suggesting that membrane tension effectively regulates the cellular uptake.

The cellular uptake also depends on the surface concentration of adhering NPs. Figure 4b plots the maximal cellular uptake for varying surface concentrations (the optimal radius is independent of surface concentration). We found that when the surface concentration is small (<0.0012), all the adhering NPs are

Table 1. Experimental/model comparisons of the optimal particle radius and the maximal cellular uptake. All the experimental data and theoretical predictions listed are based on receptor-mediated endocytosis (RME). In the work of Chithrani et al. [15], the cellular uptake depends on the types of cell lines and of the proteins coated onto the NPs. Chithrani et al. [16] also pointed out that the endocytosis of Au NPs may be clathrin-dependent. The model of Gao et al. [5], and the experiments performed by Aoyama and co-workers [12,14,26] did not report the range of cellular uptake.

Experiments/Models	R_{opt} [nm]	N_{max}	Mechanisms	Materials/Cells
Present model	~25–30	500–5000	RME	–
Gao et al. (2005)[5]	~27–30	–	RME	–
Chithrani et al. (2006)[15]	25	6160	RME	HeLa cells, SNB19, and STO cells; Au NP
Chithrani et al. (2007)[16]	25	500–3000	RME	HeLa cell; Au NP
Aoyama et al. (2003)[12,14]	~25	–	RME	HeLa cell; CdSe QD

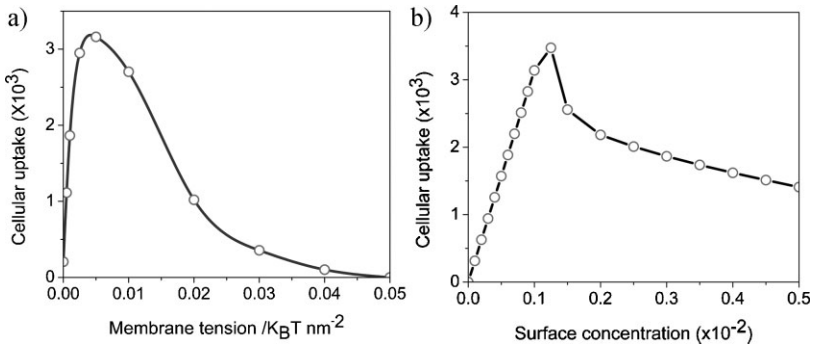

Figure 4. The effects of membrane tension and surface concentration on the cellular uptake. Simulations are performed at the optimal particle radius. a) The cellular uptake is small at extreme values of membrane tension, and remains at a high level of ~3000 within a narrow range of membrane tension. b) The cellular uptake linearly increases with increasing surface concentration, and then reaches a peak, beyond which it monotonically decreases due to the competition of receptors among NPs.

endocytosed, leading to a linear relationship between the surface concentration and the cellular uptake. As the surface concentration increases, the cellular uptake reaches a peak, and then decreases monotonically. Our calculations terminated at $c = 0.005$, because this surface concentration corresponds to a rather dense packing of NPs. The monotonic decrease of the cellular uptake with increasing surface concentration can be rationalized by the increasingly high competition for receptors among NPs. At small surface concentrations, there should be enough receptors to fully wrap *all* the NPs on the cell membrane, leading to a linear relationship between the cellular uptake and the surface concentration of NPs. As the surface concentration exceeds a critical value, the single-phase wrapping-size distribution is bound to change, since the total wrapped-membrane area is distributed to a larger number of NPs. As a result, the cellular uptake decreases.

It is worth pointing out that our prediction of the upper limit of particle radii (60 nm) for receptor-mediated endocytosis (Fig. 3) is due to the assumption of a relatively large cell-surface concentration of NPs, for which tension-mediated competition of free receptors among NPs is the governing mechanism. In the case of very low cell-surface NP concentration (i.e., only a few NPs adhere to the cell membrane), our thermodynamic model predicts that the free receptors are always excessive (from Eqs. 6–7, one notes that at this limiting case, the density of the free receptors approaches the initial receptor density), indicating that endocytosis is no longer receptor-limited. Instead, the cellular uptake in this limit is governed by the single-particle wrapping energetics. Distinct from the local energetics of wrapping a small particle, as analyzed in ref. [9], the energy of membrane tension may become dominant over the bending energy in the wrapping process of a large particle. Our analysis in the limit of very low cell-surface NP concentration shows that endocytosis can occur for very large NPs with diameters up to a few micrometers. Indeed, the microscale upper bound for particle radius for endocytosis was derived by Dietrich et al.[27] more than a decade ago.

In summary, the present study provides a thermodynamic model for the many-NP-cell system, with which we demonstrate that the cellular uptake of ligand-coated NPs is strongly size-dependent. We identified three regimes separated by two characteristic particle radii, R_{min} and R_{max}. In region I ($R < R_{min} \approx 20$ nm), endocytosis hardly occurs, because the adhesion energy is too low to compensate for the bending energy. In region III ($R > R_{max} \approx 60$ nm), endocytosis rarely occurs, and almost all NPs are only partially wrapped, because of the depletion of the free receptors. Other endocytic pathways may be active beyond these two critical radii. We rationalized the size-dependent cellular uptake by the local and global energetics of NP wrapping. For example, the upper limit of particle radius for endocytosis can be a few micrometers when the surface NP concentration is very low. In region II ($R_{min} < R < R_{max}$), an optimal NP radius is identified at which the cellular uptake of NPs is maximized. The optimal radius falls in the range of 25–30 nm for reasonable values of the membrane bending rigidity and the ligand–receptor binding energy. Accordingly, the maximal cellular uptake ranges from 500 to 5000. Both the optimal radius and the cellular uptake agree satisfactorily with the available experimental data.[12,14,15,16]

We also investigated the effects of membrane tension and of the surface concentration of NPs on the cellular uptake. Our model predicts an optimal surface concentration beyond which the cellular uptake decreases due to the competition of receptors among NPs. The model also suggests that membrane tension regulates the cellular uptake. We point out, however, that our model may overestimate the membrane tension effect, especially when other mechanisms, including clathrin-coat and lipid insertion, are active. During endocytosis, wrapping of NPs may proceed by insertion of lipids from cytoplasm into highly curved regions (the bound regions) rather than by laterally pulling the lipids,[28] which effectively lowers the stretching energy Γ_k. In addition, membrane curvature formation generally couples with the concentration of different lipid compositions at the highly curved regions,[29] which also lowers the deformation energy Λ_k of the free membrane detaching from the NP. Furthermore, NP wrapping may activate the release of local membrane reservoirs, which also lowers the work required to wrap the NP. These effects lower the tension-mediated energy barrier, giving rise to a larger R_{max}.

The present study addresses the question of ''how many'' NPs can be internalized into the cell upon attaining a thermodynamic equilibrium. The model introduced in this work provides valuable insight into the steady-state cellular uptake observed in the experiments. Our thermodynamic approach is distinctly different from the kinetic model developed by Gao et al.,[7] in which the endocytic time of a single NP is of interest. Interestingly, the optimal particle radius for maximal cellular uptake predicted by our thermodynamic model is fairly close to the value corresponding to the shortest endocytic time found by the kinetic model of Gao et al.,[7] and consistent with the analytic solution of R_{min} presented in Bao and Bao.[9] Taken together, the uptake rate reaches a maximum at the optimal radius of ~25 nm, which provides a valuable piece of information for the rational design of NP-based cellular delivery. The optimal radius also falls in the size

range of typical viruses, manifesting broad implications of materials design principles exploited by nature via evolution. The predicted maximal cellular uptake of NPs is also valuable for assessing NP toxicity, the efficiency of NP-based bioimaging and biomarkers, and the therapeutic efficacy of NP-based drug carriers.

Experimental

Numerical scheme: The numerical scheme we followed to compute the cellular uptake as a function of particle radius, membrane tension, and surface concentration of the NPs is presented here. The thermodynamic equilibrium of the NP–cell system can be found by minimizing the total free energy functional Equation 3 with respect to L_b and n_k. Minimizing the free energy functional with respect to L_b yields,

$$\frac{\xi_f}{1-\xi_f} = e^{-\mu}\frac{\xi_b}{1-\xi_b} \tag{4}$$

while minimizing the free energy functional with respect to n_k in combination with the conjugate condition described in Equation 1 gives rise to the normalized wrapping size distribution p_k, i.e., the fraction of NPs with a wrapped area of k,

$$p_k = \frac{n_k}{N} = \frac{e^{-\beta_k}\alpha^k}{\sum_{k=0}^{K} e^{-\beta_k}\alpha^k}, \tag{5}$$

where $\alpha = (\xi_f/\xi_b)e^{\mu-\hat{\kappa}}$ and $\beta_k = \Gamma_k + \Lambda_k + 4\pi\overline{\kappa}\delta_{kK}$, where δ_{kK} is the Kronecker delta function. The conservation condition of the receptors yields:

$$\varphi_f\xi_f + \varphi_b\xi_b = \xi_0, \tag{6}$$

where φ_f and φ_b are the area fraction of free and bound membrane surfaces, respectively. Note that $\varphi_f = 1-\varphi_b$, and

$$\varphi_b = c\sum_{k=0}^{K} kp_k. \tag{7}$$

The densities of the free and bound receptors ξ_f and ξ_b, respectively, can be obtained by solving the combined Equations 4–7. The nonlinear equations can be most conveniently solved by the false-position method, as it does not involve computations of derivatives. Substituting ξ_f and ξ_b back into Equation 5 yields the wrapping-size distribution, and hence the number of fully internalized NPs

$$n_K = cMp_K \tag{8}$$

where p_K is the uptake ratio.

Acknowledgements

S. Z. acknowledges support from the National Science Foundation (NSF) grant CMMI-0754463. J. L. acknowledges support from NSF, AFOSR, ONR, and Ohio Supercomputer Center. G. L. and S. S. acknowledge support from the Computational Systems Biology Programme and Advanced Materials for Micro and Nano Systems Programme of the Singapore-MIT Alliance and the Interdisciplinary Research Group on Infectious Diseases funded by the Singapore-MIT Alliance for Research and Technology. GB acknowledges support from the National Heart Lung and Blood Institute of the NIH through the Program of Excellence in Nanotechnology grant (HL80711). We thank Huajian Gao and K. Jimmy Hsia for helpful discussions. This article is part of a Special Issue on Biomaterials.

Received: May 20, 2008
Revised: July 23, 2008
Published online: November 18, 2008

[1] O. Veiseh, C. Sun, J. Gunn, N. Kohler, P. Gabikian, D. Lee, N. Bhattarai, R. Ellenbogen, R. Sze, A. Hallahan, J. Olson, M. Q. Zhang, *Nano Lett.* **2005**, *5*, 1003.
[2] R. Duncan, L. Izzo, *Adv. Drug Delivery Rev.* **2005**, *57*, 2215.
[3] J. K. Jaiswal, E. R. Goldman, H. Mattoussi, S. M. Simon, *Nat. Methods* **2004**, *1*, 73.
[4] X. Michalet, F. F. Pinaud, L. A. Bentolila, J. M. Tsay, S. Doose, J. J. Li, G. Sundaresan, A. M. Wu, S. S. Gambhir, S. Weiss, *Science* **2005**, *307*, 538.
[5] Y. W. C. Cao, R. C. Jin, C. A. Mirkin, *Science* **2002**, *297*, 1536.
[6] R. Elghanian, J. J. Storhoff, R. C. Mucic, R. L. Letsinger, C. A. Mirkin, *Science* **1997**, *277*, 1078.
[7] H. J. Gao, W. D. Shi, L. B. Freund, *Proc. Natl. Acad. Sci. USA* **2005**, *102*, 9469.
[8] D. M. Lerner, J. M. Deutsch, G. F. Oster, *Biophys. J.* **1993**, *65*, 73.
[9] G. Bao, X. R. Bao, *Proc. Natl. Acad. Sci. USA* **2005**, *102*, 9997.
[10] S. Tzlil, M. Deserno, W. M. Gelbert, A. Ben-Shaul, *Biophys. J.* **2004**, *86*, 2037.
[11] D. van Effenterre, D. Roux, *Europhys. Lett.* **2003**, *64*, 543.
[12] Y. Aoyama, T. Kanamori, T. Nakai, T. Sasaki, S. Horiuchi, S. Sando, T. Niidome, *J. Am. Chem. Soc.* **2003**, *125*, 3455.
[13] T. Nakai, T. Kanamori, S. Sando, Y. Aoyama, *J. Am. Chem. Soc.* **2003**, *125*, 8465.
[14] F. Osaki, T. Kanamori, S. Sando, T. Sera, Y. Aoyama, *J. Am. Chem. Soc.* **2004**, *126*, 6520.
[15] B. D. Chithrani, A. A. Ghazani, W. C. W. Chan, *Nano Lett.* **2006**, *6*, 662.
[16] B. D. Chithrani, W. C. W. Chan, *Nano Lett.* **2007**, *7*, 1542.
[17] X. L. Xing, X. X. He, J. F. Peng, K. M. Wang, W. H. Tan, *J. Nanosci. Nanotechnol.* **2005**, *5*, 1688.
[18] W. Helfrich, *Z. Naturforsch. C* **1973**, *C28*, 693.
[19] M. Deserno, T. Bickel, *Europhys. Lett.* **2003**, *62*, 767.
[20] H. Garoff, R. Hewson, D. J. E. Opstelten, *Microbiol. Mol. Biol. Rev.* **1998**, *62*, 1171.
[21] D. L. Nelson, M. M. Cox, *Lehninger Principles of Biochemistry*, W. H. Freeman, 4th ed. New York **2004**.
[22] J. A. G. Briggs, T. Wilk, S. D. Fuller, *J. Gen. Virol.* **2003**, *84*, 757.
[23] P. Quinn, G. Griffiths, G. Warren, *J. Cell Biol.* **1984**, *98*, 2142.
[24] G. Apodaca, *Am. J. Physiol.-Renal Physiol.* **2002**, *282*, F179.
[25] M. P. Sheetz, *Nat. Rev. Mol. Cell Biol.* **2001**, *2*, 392.
[26] M. P. Desai, V. Labhasetwar, E. Walter, R. J. Levy, G. L. Amidon, *Pharm. Res.* **1997**, *14*, 1568.
[27] C. Dietrich, M. Angelova, B. Pouligny, *J. Phys. II* **1997**, *7*, 1651.
[28] K. N. J. Burger, R. A. Demel, S. L. Schmid, B. de Kruijff, *Biochemistry* **2000**, *39*, 12485.
[29] H. T. McMahon, J. L. Gallop, *Nature* **2005**, *438*, 590.